Effect of γ-Radiation on Electrical and Magnetic Properties of Manganite Materials with Spinel Structures

M. Khairy*, **M. A. Mousa**

Chemistry Department, Faculty of Science, Benha University, Benha, Egypt

Abstract   Nano $Co_{0.1}Zn_{0.9}Mn_2O_4$ samples were prepared by hydrothermal method in absence and presence of surfactants. The samples were characterized using XRD, SEM and TEM. Magnetic and electrical properties (DC- and AC-conductivity) were studied. Influences of gamma radiation on the properties studied were investigated. All samples showed tetragonal spinel crystal structure with morphologies and crystallites sizes depending on the preparation method and lay in the range of 11- 72 nm. The conductivity results showed semiconducting behavior for the samples investigated and were explained by hopping mechanism in which the conduction occurred via electron exchange amongst transition metal ions situated on octahedral sites in spinel lattice. Room temperature magnetic properties using VSM were studied. The physical properties studied were found to be dependent on the type of surfactants used.

Keywords   Nano-Manganate, Surfactants, Γ-Irradiation, Magnetic Properties , Electrical Conductivity

1. Introduction

Nanomaterials are structures with dimensions characteristically between 1 and 100 nm; when engineered appropriately, these materials exhibit a variety of unique and tunable chemical and physical properties compared to those of bulk.

They are revolutionizing a wide range of fields and applications by allowing control of materials structure at the molecular scale and they have become a symbol of the new and fast developing research area of nanotechnology. The field of nanoscience has undergone unprecedented growth during the last few years and has received a great deal of attention. Significant enhancement of optical, mechanical, electrical, structural, and magnetic properties are commonly found through the use of novel nanomaterials[1].

Among various nanomaterials, magnetic nanoparticles mainly spinel mixed transition metal oxides nanoparticles, are of special interest for their attractive scientific and technological aspects in different fields such as electronic[2], magnetic recording[3], solid batteries[4], catalyst[5], photocatalyst[6], drug delivery[7], pigments[8], ferrofluids[9], magnetic resonance imaging (MRI)[10]…….etc. These materials crystallize in the spinel structure, that is a cubic close packing of oxygen anions in which the cations are located on the tetrahedral sites (A) and the octahedral sites (B)[11].

There are many methods for the preparation of nanocrystalline spinels, like sol–gel method[12], thermal decomposition[13], solid state reaction[14], microwave heating[15] , coprecipitation[16]or mechanical milling and mixing of respective oxides[17]. General approaches for shape control and production of anisotropic nanostructures rely on the availability of surfactants, which preferentially absorb on specific crystallographic faces. With ever increasing energy costs, the hydrothermal method may be better used for fine powder preparation because of the low temperature involved, crystal size and the morphology of the powders can be controlled by reaction conditions[18].

Complex manganese oxides have recently evoked strong interest in various structures with different Mn valence states and Mn coordination for example in perovskites, or spinels. The manganites display a vast range of fascinating catalytic, electrical and magnetic properties, which often come about due to the mixed valence states of manganese[19-21].

As a part of our program to prepare and study physical properties of nano pure and doped $ZnMn_2O_4$; this work was designed to prepare nanosized $Co_{0.1}Zn_{0.9}Mn_2O_4$ which is a member of mixed transition-metal oxides by hydrothermal method in absence and in presence of different surfactants. The materials obtained were characterized by X-ray diffraction (XRD), scanning electron microscopy (SEM) and transmission electron microscopy (TEM). Electrical conductivity as well as magnetic properties of the produced materials were studied. The effects of γ-irradiation on the studied properties were also investigated.

2. Experimental

* Corresponding author:
moh_khairy3@yahoo.com (M. Khairy)

2.1. Materials

All the chemical reagents used in the experiment were A.R. grade and used without further purification and treatment. The surfactants used in the preparation method were divided into three different groups: (a) Cationic surfactants: cetyltrimethyl ammonium bromide monohydrate (CTAB)$\{CH_3(CH_2)_{15}N(CH_3)_3Br\}$ (98%) provided from Aldrich; (b) Anionic surfactants: dodecylbenzene sulphonic acid (Sulph) $\{CH_3(CH_2)_{11}C_6H_4SO_3H\}$ provided from chemicals and dyes company, Kafr El Doar and (c) Nonionic surfactants: triton X-100 (TX) $\{C_{14}H_{22}O(C_2H_4O)_n\}$ provided from Arsamco.

2.2. Sample Preparation

A mixed solution of 1 ml H_2O_2 (3%) and 6 ml NaOH (0.6 M) was poured slowly into a Teflon-lined stainless-steel autoclave filled with 3 ml $Mn(NO_3)_2$ (0.3 M) while stirring vigorously, and the reaction solution was continually stirred and kept for 20 min. at the room temperature. Suitable amounts $Zn(NO_3)_2 \cdot 6H_2O$ (GFS Chemicals) were mixed to $Co(NO_3)_2 \cdot 6H_2O$ (Carlo Erba) in 250 ml of distilled water. Then, metal of zinc and cobalt (II) in the Co/Co+Zn molar ratio of 0.1 was added with the surfactant into the reaction solution. After this the reaction solutions were hydrothermally heated at 200℃ for four days. The samples prepared hydrothermally were cooled to room temperature, then the precipitates were filtered and washed with distilled water several times until pH=7, and finally dried in an oven at 90℃.

Half of the prepared samples was irradiated by γ-ray source using a ^{60}Co gamma cell (^{60}Co gamma cell 2000 Ci with a dose rate of 1.5 Gy/s (150 rad/s) at a temperature of 30℃. Each samples was subjected to a total final dose of 1×10^5 Gy (10 Mrad).

The prepared samples are denoted as Z, Z_{CTAB}, $Z_{TX,}$ and Z_{sulph} for the samples prepared without surfactant and by using CTAB, TX, and sulph surfactants, respectively. The γ-irradiated samples will be denoted by *.

2.3. Techniques

X-ray diffraction were performed on the investigated samples using a Philips X'Pert Pro Super diffractometer with Cu Kα radiation (λ = 1.54 Å) in the range of 2θ = 10 - 80^0. The density was determined by both the immersion Archimedes method and X-ray diffraction. Electron microscopes analysis using SEM and TEM were taken by an electron microscope model JEM-5200 Joel and Joel 2010, respectively.

For electrical measurements, the powder samples were pressed uniaxially into a pellet of thickness 1–2 mm and of diameter 7 mm by applying pressure of ~ 0.3 Gpa for 3 min. Both faces of the pellets were coated with fine quality silver paint for good electrical contacts. DC conductivity was measured in the temperature range 300-400 K by the four terminal technique. The temperature was limited to 400 K to prevent grain growth and to ensure that the main particle size remained the same in the entire temperature range. AC-conductivity was measured by the two-probe method using Fluke PM 6306 programmable automatic (RCL) bridge at frequencies from 10^2–10^6 Hz over the same temperature range used in dc-measurements.

3. Results and Discussion

3.1. X-Ray Diffraction

X-ray diffraction patterns of the investigated samples are presented in Fig. 1. For all samples the same patterns were observed with well developed (h *k l*) reflections, which can be well indexed on the basis of the tetragonal spinel structure with the space group of Fd-3m[22]. No trace of impurity phases of starting materials is observed in the present patterns, indicating the formation of single – phase tetragonal spinel compounds.

The parent component of $ZnMn_2O_4$ show spinel lattice consist of O^{2-} anions form a close-packed tetragonal lattice in which the Zn^{2+} are located in tetrahedral sites (labeled as A sites) and Mn^{3+} cations are located in octahedral sites (labeled as B sites)[23]. The $Co_{0.1}Zn_{0.9}Mn_2O_4$ samples crystallize also as spinel with a unit cell (~299.00 A^3) smaller than that of $ZnMn_2O_4$ (301.22 A^3)[24]. This indicates that Co^{3+} ions partially replacing the Mn^{3+} ions in the octahedral sites[22].
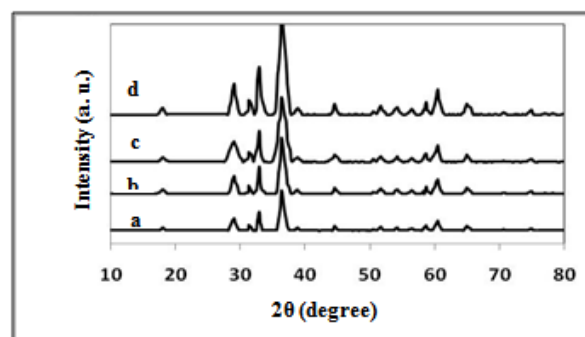
(b)
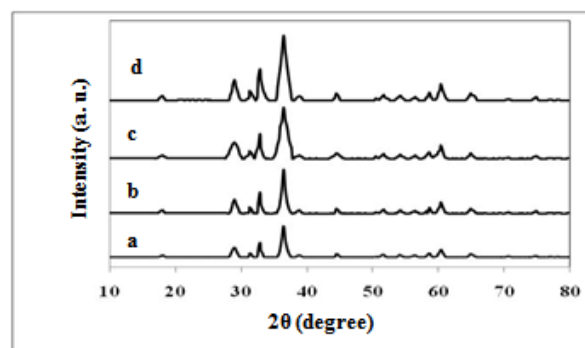
(a)

Figure 1.   (a) XRD patterns for unirradiated samples: a) Z_{sulph}, b) Z, c)Z_{TX}, d)Z_{CTAB} (b) XRD patterns for γ-irradiated samples: a) Z^*_{sulph}, b) Z^*, c)Z^*_{TX}, d)Z^*_{CTAB}

Table 1. Lattice parameters, density and porosity of investigated $Co_{0.1}Zn_{0.9}Mn_2O_4$ samples

Sample	Lattice constant(nm)	Volume of Unit Cell x10^{22} m^3	d_{XRD} g/cm^3	d_A g/cm^3	D_{TEM} (nm)	D_{XRD} (nm)	P%
Z_{sulph}	a=0.569,c=0.918	2.972	5.332	3.999	11	13	25.0
Z^*_{sulph}	a=0.570,c=0.919	2.986	5.307	3.874	15	17	26.9
Z	a=0.570,c=0.919	2.985	5.309	4.141	35	33	22.1
Z^*	a=0.571,c=0.920	2.999	5.284	3.974	44	42	24.8
Z_{TX}	a=0.571,c=0.920	2.999	5.284	4.222	59	62	20.1
Z^*_{TX}	a=0.572,c=0.921	3.013	5.259	4.076	68	72	22.5
Z_{CTAB}	a=0.572,c=0.921	3.013	5.259	4.276	32(diam)	50	18.7
Z^*_{CTAB}	a=0.572,c=0.922	3.017	5.252	4.322	33(diam)	51	17.7

The size of the particles was determined from the diffraction peaks broadening with the use of the Debye-Scherrer equation[25]:

$$D_{XRD} = 0.9\lambda / \beta \cos\theta \qquad (1)$$

Where λ is the wavelength of X-ray; β is the full width at half maximum and θ is the Bragg's diffraction angle. The crystallites sizes of the samples under investigation are presented in Table 1.

Table 1 shows that the samples irradiated with high energetic γ-rays have larger particle sizes than that of untreated ones. The irradiation may cause splitting in crystal lattice[26] and producing oxidation - reduction in the cations present in the lattice (see later). All these processes induce lattice sites which favors the formation of large crystals[26, 27].

The X-ray density of all the compositions was calculated using the formula:

$$d_{XRD} = Z'M / NV \qquad (2)$$

Where Z' is the number of molecules per unit cell ($Z' = 4$); M is the molecular weight; N the Avogadro's constant and V is the volume of unit lattice.

The bulk density (d_A) was also measured by the Archimedes principle. The percentage porosity (P) of the samples was then calculated using the relation:

$$P = (1 - d_A/d_{XRD}) \times 100 \qquad (3)$$

The values of the bulk density and porosity are both tabulated in Table 1. From the table it is clear that the porosity increases with decreasing the grain size, except for the Z_{CTAB} sample, according to the order:

$$Z_{sulph} > Z > Z_{TX} > Z_{CTAB}$$

3.2. SEM and TEM

The morphology and the particle size of the powdered samples are investigated using scanning electron micrographs (SEM) and transmission electron images (TEM). The analysis of images obtained (Fig. 2) reveals that the morphology of the prepared particles depends to a large extent on the type of surfactant used in the preparation method. Where, the micrographs of the sample prepared in absence of surfactant (Z) showed large grains with particles do not have a well-defined morphology. On the other hand, the samples prepared using CTAB surfactant (Z_{CTAB}) showed the formation of nano rods particles. CTAB has been

worked here as a morphology directing agent. CTAB has been also successfully used as the morphology-directing agent for the synthesis of one-dimensional nanostructures, such as CuO, PbO_2, Pb_3O_4 and Co_3O_4 nanorods[28-29].

(b)

(a)
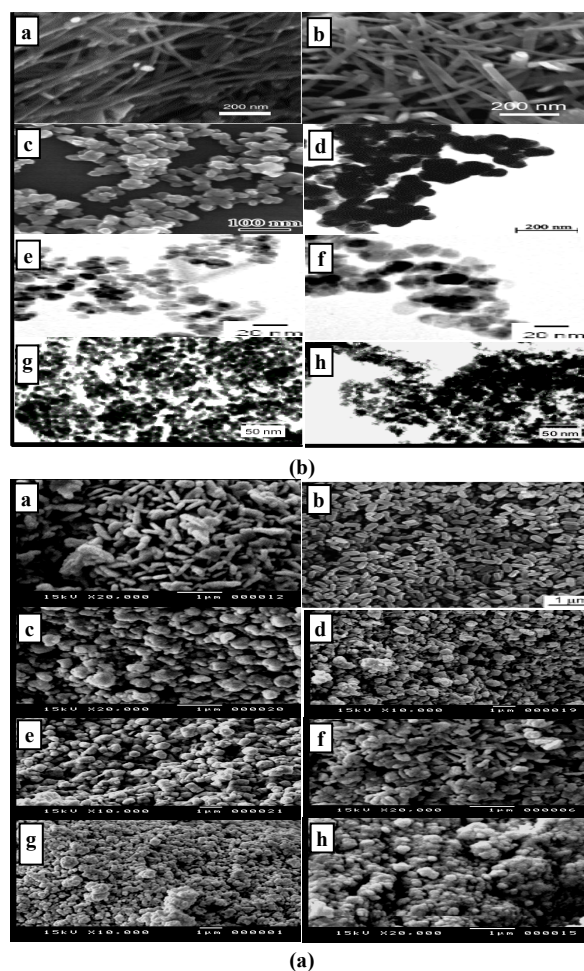
Figure 2.   (a) SEM: a) Z_{CTAB}, b) Z^*_{CTAB}, c) Z_{TX}, d) Z^*_{TX}, e) Z_{sulph}, f) Z^*_{sulph}, g) Z, h) Z^*. (b) TEM: a) Z_{CTAB}, b) Z^*_{CTAB}, c) Z_{TX}, d) Z^*_{TX}, e) Z_{sulph}, f) Z^*_{sulph}, g) Z, h) Z^*

This can be explained on the basis of the[29] electrostatic interactions occurring between the inorganic precursor and the cationic surfactant CTAB to form inorganic–surfactant composite templates. In the tetragonal spinel, the growth direction of the $Co_{0.1}Zn_{0.9}Mn_2O_4$ nanorods can be determined as the[111] crystallographic direction. However, the images

analysis of other samples prepared using anionic surfactant (sulph) or non-ionic surfactant (TX) showed, on the other hand, nano particles with different shapes, Fig. 2. More image analyses showed surface morphologies for the irradiated samples differ to some extent than that of unirradiated ones. Furthermore, the pores sizes became larger after irradiation process. This indicates that the high ionization radiation produced an effect on the surface of the sample. The mean grain sizes using TEM analysis (D_{TEM}) differs to some extent than D_{XRD}, Table 1. This may be attributed to either the presence of non-crystalline materials at the lattice surface or to the different approach of two techniques.

In XRD, the estimated crystal size showed the average size of the crystals, and the accuracy of the Scherrer equation is affected by many factors such as diffraction line width, defects, surface tension, so the Scherrer formula may induce some errors in measuring the absolute values of the crystallite size

3.3. Electrical Properties

The dc-conductivity (σ_{dc}) of the $Co_{0.1}Zn_{0.9}Mn_2O_4$ samples are evaluated using the relation

$$\sigma_{dc} = l/R_{dc}A \qquad (4)$$

Where R_{dc} is the dc resistance, l is the thickness, and A is the area of the electrode deposited on the sample. According to the ionic radius of the different cations present in $Co_{0.1}Zn_{0.9}Mn_2O_4$, the electrical conduction is possible only if some different oxidation states are present on the octahedral sites of the spinel structure. Thus, due to the electronic configuration ($3d^{10}$), the Zn^{2+} cations are highly stabilized on the tetrahedral sites of the spinel structure[30]. And because the ionic radius of Co^{2+} is very close to that of Zn^{2+}[31], therefore the $Zn_{0.9}^{2+}Co_{0.1-3y}^{2+}[Co_{2y}^{3+}Mn_{2(1-2x)}^{3+}Mn_{3x}^{+4}]O_4$ formula is used to explain the conductivity results. It should be mentioned here that the large distances between the ions present on tetrahedral sites (compared with that found in octahedral sites) decrease the effective contribution of these ions in the conduction process. Therefore, the hopping phenomena between Mn^{3+} and Mn^{4+} is responsible for the electrical conduction in the investigated system. It should be also mentioned that the hopping of electrons between different transition state ions is less predominant than that of the same metal ions[32].

The temperature dependence of dc-conductivity showed a thermal activation process, Fig. 3, which can be explained according to:

$$\sigma_{dc} = \sigma_0 \exp(-E_{dc}/kT) \qquad (5)$$

where σ_0 is the pre-exponential factor, E_{dc} is the activation energy and k is the Boltzmann constant. From the slopes of the plots the activation energies E_{dc} have been calculated and listed in Table 2. It is evident to see that the conductivity changes with each of the morphology and the particle size of the investigated samples. Where, the conductivity decreases with decreasing the particle size, except for the nanorods S_{CTAB} sample. The nano sample introduces grain-boundaries

in material and its volume fraction is much more with decreasing the particle size. This is attributed mainly to the spatial confinement of free and bound charges, and disorder grain boundary. It is well known that the grain boundaries in nanocrystalline materials exhibit a random atomic arrangement without short or long range order[33]. Moreover, it is known that the diffusion through grain-boundaries is much faster than grain-interior diffusion hence large volume fraction of grain-boundary plays a dominant role in conduction. This can be attributed to the change in the concentration of charge carrier with each of the change in the morphology and the particle size of $Co_{0.1}Zn_{0.9}Mn_2O_4$.
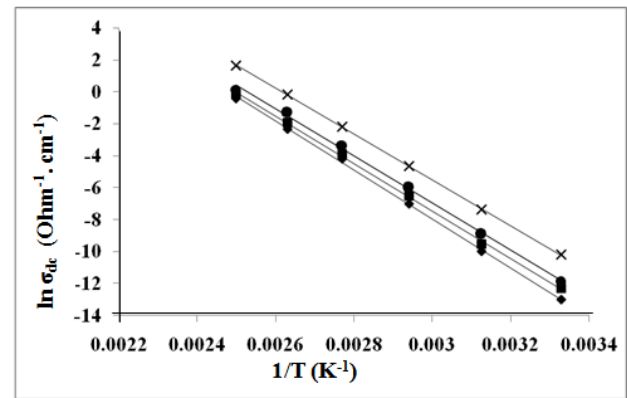
Figure 3. The temperature dependence of DC-conductivity for: (♦), Z_{Sulph}; (■). Z; (●), Z_{TX}; (×), Z_{CTAB}

Table 2. Conductivity data of γ-irradiated and unirradiated $Co_{0.1}Zn_{0.9}Mn_2O_4$ samples at 300 K

Sample	Particle Size (nm)	σ (ohm⁻¹.cm⁻¹)	E_{dc} (eV)
Z^*_{sulph}	17	[5.2x10⁻⁶]	[1.36]
Z_{sulph}	13	2.2x10⁻⁶	1.31
Z^*	42	[9.1x10⁻⁶]	[1.28]
Z	33	4.5x10⁻⁶	1.25
Z^*_{TX}	72	[1.2x10⁻⁵]	[1.27]
Z_{TX}	62	6.79x10⁻⁶	1.21
Z^*_{CTAB}	51	[6.11x10⁻⁵]	[1.11]
Z_{CTAB}	50	3.71x10⁻⁵	1.05

[   ] irradiated data

The γ-irradiated samples showed a slight change in the activation energy values and an increase in the electrical conductivity comparable with that found for the unirradiated ones. This influence of gamma radiation may be attributed to the following ionization process that occurring for the different transition metal ions: $\gamma + M^{n+} \rightarrow M^{n+1} + e$

This interaction leads to a change in each of the amount and the distribution of transition metal ions on both octahedral and tetrahedral sites. The almost non change in activation energy values (before and after irradiation process) refers to a non change in the conduction mechanism. But the increase in conductivity values after irradiation refers to the change occurring in the redox ratio on the octahedral sites which causes an increase in the hopping rate and in turn the conductivity values, as shown in our results

In order to give information on the type of polarization present in the samples, the ac-electrical conductivity (σ_{ac}), at temperatures between 300 - 400 K and at frequency range of $10^2 – 10^6$ Hz was studied. The ac-conductivity σ_{ac} (ω) was calculated by subtracting the measured dc-conductivity (σ_{dc}) from the measured total frequency-dependent conductivity σ_{ac} (ω) such that

$$\sigma_{ac} = \sigma_t - \sigma_{dc} \qquad (6)$$

Fig. 4, displays the ac-conductivity as a function of frequency at different temperatures for unirradiated samples. The same variation is also observed for irradiated samples with different particle sizes. For all samples, the ac-conductivity increases with increases the temperature; referring to the semiconductor nature of the samples, as commonly seen in most similar transition metal oxides with spinel structure. The increase of σ_{ac} is attributed to the increase in the drift mobility and hopping frequency of charge carriers with increasing temperature. Generally, it can be said that the studied samples shows a semi-conducting trend, as commonly seen in most transition metal oxides. Like insulators and many semi-conductors the ac-conductivity, at lower temperatures, follows the equation[34].
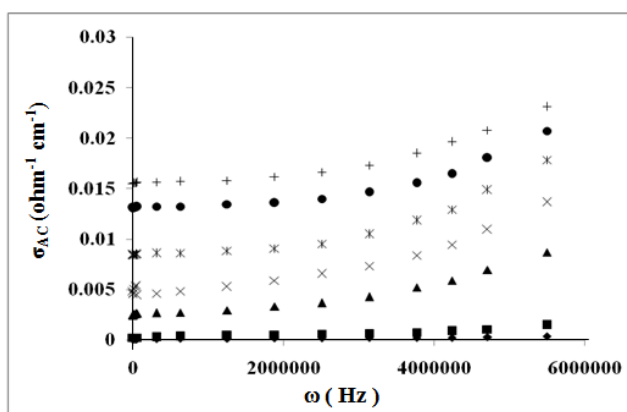
Figure 4. The frequency dependence of AC-conductivity for: (♦), $Z_{(Sulph)}$; (■), Z; (▲), Z_{TX}; (x), Z_{CTAB}(300K); (✹), Z_{CTAB}(340K); (●), Z_{CTAB}(380K); (+), Z_{CTAB}(400K)

$$\sigma_{ac} = A\omega^s \qquad (7)$$

where A is a constant dependent on temperature and s is the frequency exponent. The power s in Eq. (7) is deduced at different ambient temperatures for the material investigated and s was found to lie in the range 0.1- 0.60 and decreases with increasing temperature. The s values for irradiated samples are lower than that for unirradiated ones. The activation energy for conduction process decreases with increasing frequency. Generally, in the dc conductivity the charge carriers choose the easiest path between the ions. These paths will include some jumps for which R, the distance between the ions, is large. This is not so important in the ac conduction. Thus low activation energy may be involved in the ac conduction. The difference between the activation energies of σ_{dc} and σ_{ac} may be attributed to the effective drop of the electric field within the bulk due to the

presence of space charge accumulations at the electrodes which were noticed in dc-measurements[35].

3.4. Magnetic Properties

Vibrating sample magnetometer (VSM) was used to investigate the magnetic properties of γ-irradiated and unirradiated $Co_{0.1}Zn_{0.9}Mn_2O_4$ at room temperature. All samples showed narrow hysteresis loops, indicating their slight ferromagnetism. Typical plot is shown in Fig. 5. The irradiated ones showed the same behavior. The saturation magnetizations Ms of the samples were obtained by extrapolating M vs. 1/H plot to 1/H=0. The variation trend of Ms, Hc and Mr was illustrated in Table 3. From which it can be seen that magnetization (Ms) values for irradiated are higher than unirradiated ones and increase in the following order: $Z_{CTAB} > Z_{TX} > Z > Z_{sulph}$. The ferromagnetic properties of studied samples were attributed to the simultaneous presence of different valence states of Mn ions. They give rise to ferromagnetism via the double-exchange mechanism. Zinc ions act as the retardant of the magnetic interaction between the manganese ions. The increase in ferromagnetic character of the samples by irradiation, Table 3, may be attributed to the change occurring in the ratio of oxidizing and reducing amount of Mn- and Co-ions comparable with that present in unirradiated ones, as mentioned above. The nanorod sample S_{CTAB} exhibit saturation magnetization (M_s) value, which is higher than that of other samples. This increase in magnetic properties may be strongly dependent on the growth direction of[110] which is one of the easiest magnetization in the spinel system[36]. Similar results were also found with Fe_2O_3 nanowires[37].

The increase observed in saturation magnetization with the increase in particle size, Table 3, is attributed to the nature of ultrafine particles, including the surface disorder and surface spin canting due to large surface to volume ratio for nano particular system[38, 39]. This may be also attributed to different mechanisms, such as the existence of a magnetically dead layer on the particles surface, the existence of canted spin or the existence of a spin glass like behavior of the surface spins[36],[38-40].
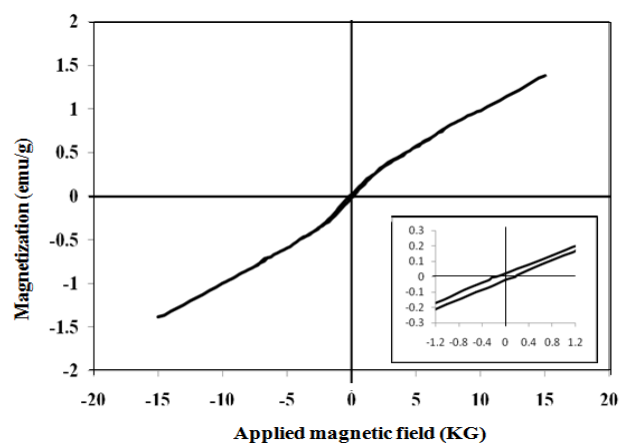
Figure 5. Room temperature magnetic hysteresis loop of Z sample. The inset is the enlargements of the center part of the curves

Table 3.   Magnetic Properties Parameters of $CO_{0.1}Zn_{0.9}Mn_2O_4$

Sample	Magnetization (Ms, emu/g)	Coercivity (Hc, G)	Residual magnetization (Mr, emu/g)
Z_{sulph}	0.19	68	0.007
Z^*_{sulph}	[0.30]	[89]	[0.011]
Z	0.45	93	0.012
Z^*	[0.57]	[110]	[0.013]
Z_{TX}	0.86	114	0.014
Z^*_{TX}	[0.98]	[128]	[0.016]
Z_{CTAB}	1.06	132	0.017
Z^*_{CTAB}	[1.38]	[170]	[0.021]

[   ] irradiated data

4. Conclusions

    Nanocrystalline $Co_{0.1}Zn_{0.9}Mn_2O_4$ were prepared in the range of 11-72 nm using hydrothermal method in presence and absence of surfactants. XRD showed a tetragonal spinel structure for the γ- irradiated and unirradiated samples. The size of the prepared particles has been confirmed through X-ray diffraction and TEM techniques. SEM and TEM images showed surface and particle morphology depends on each of the type of surfactants used and irradiation process. The porosity became also smaller after γ-irradiation process. Both ac- and dc- conductivity follows Arrhenius-type thermally activated conduction over temperature range investigated and referring to a semiconducting behavior for the γ- irradiated and unirradiated nano $Cu_{0.1}Zn_{0.9}Mn_2O_4$ samples. The irradiation process causes an increase in the conductivity values. Hopping mechanism between different oxidation states of Mn-ions in the $Zn_{0.9}{}^{2+}Co_{0.1-3y}{}^{2+}[Co_{2y}{}^{3+}Mn_{2(1-2x)}{}^{3+}Mn_{3x}{}^{+4}]O_4{}^{-}$ samples is used to explain the conducting behavior. All studied samples showed ferromagnetic behavior which increases with increasing each of the particle size and irradiation process. The relation between morphology (nanorod) and each of electrical and magnetic performance is observed.

REFERENCES

[1] T. R. H. Cutmore, D. A. James, J. Psychophysiology, 21 (1) (2007) 51.

[2] S. Banerjee, D. Bhattacharyya, Comput. Mater. Sci., 44 (1) (2008) 41.

[3] M.S. Martín-González, F. Briones, J.M. García-Martín, J. Montserrat, L. Vila, G. Faini, A.M. Testa, D. Fiorani, H. Rohrmann , J. Mag. Mag. Mater., 322 (18) (2010) 2762.

[4] F. Liu, R. Kirchheim, J. Cryst. Growth, 264(1-3) (2004) 385

[5] G. Ferraris, G. Fierro, M. Lo Jacono, M. Inversi, R. Dragone, Appl. Catal. B: Envir., 36 (4) (2002) 251.

[6] P. Guo, X. Wang, H. Guo. Appl. Catal. B: Envir., 90 (3-4) (2009) 677.

[7] L. C. du Toit, V. Pillay, Y. E. Choonara, Adv. Drug Deliv. Rev., 62(4-5) (2010) 532.

[8] P. M. T. Cavalcante, M. Dondi, G. Guarini, M. Raimondo, G. Baldi , Dyes and Pigm., 80(2) (2009) 226.

[9] T. H. Tsai, D. S. Liou, L. S. Kuo, P. H. Chen, Sen. and Act. A: Physical, 153 (2) (2009) 267.

[10] H. Yang, Y. Zhuang, Y. Sun, A. Dai, X. Shi, D. Wu, F. Li, H. Hu, S. Yang, Biomat., 32 (20) (2011) 4584.

[11] A.C.F.M. Costa, A.M.D. Leite, H.S. Ferreira, R.H.G.A. Kiminami, S. Cava, L. Gama J. Eur. Ceramic Soc. 28 (2008) 2033.

[12] S. M. H. Hejazi, F. Majidi, M. P. Tavandashti, M. Ranjbar , Mater. Sci. Semi. Process., 13 (4) (2010) 267.

[13] E. Darezereshki, Mater. Lett., 65 (4) (2011)642.

[14] X. Chu, S. Zhou, W. Zhang, H. Shui , Mater. Sci. and Eng.: B, 164(1) (2009) 65.

[15] X. Chu, Y. Han, S. Zhou, H. Shui, Ceram. Intern., 36(7) (2010) 2175.

[16] Y. Xu, X. Liu, Y. Ding, L. Luo, Y. Wang, Y. Zhang, Y. Xu, Appl. Clay Sci., 52 (3) (2011)322.

[17] A. Charkhi, H. Kazemian, M. Kazemeini, Powd. Techn., 203(2) (2010) 389.

[18] Y. B. Kwon, S. W. Shin, H. Lee, J. Y. Lee, J. Moon, J. Kim, Cur. Appl. Phys., 11(1) (2011) S197.

[19] S. G. Fritsch, C. Chanel, J. Sarrias, S. Bayonne, A. Rousset, X. Alcobe, M. L. Martinez Sarriòn, Solid State Ionics, 128 (1-4) (2000) 233.

[20] G. Ferraris, G. Fierro, M. Lo Jacono, M. Inversi, R. Dragone, Appl. Catal. B: Envir., 36 (4) (2002) 251.

[21] F. Liu, R. Kirchheim, J. Cryst. Growth,264(1-3) (2004) 385

[22] G. Fierro, M. Lo Jacono, M. Inversi, R. Dragone and G. Ferraris. Appl. Catal. B: Envir. 3 (2001) 173.

[23] S.T. Kshirsagar, A.B. Biswas, J. Phys. Chem. of Solids, 28 (8) (196) 1493.

[24] M. Nogues and P. Poix. C.R. Acad. Sc. (Paris), 272 (1971) 1318.

[25] H. P. Klug, L.E. Alexander, X-ray diffraction procedures, Wiley, New York (1970).

[26] H.G. El-Shobaky, W.M. Shaheen Radiation Physics and Chemistry 66 (2003) 55.

[27] Y. Liu, Y. Zhang, M. Zhang, W. Zhang, Y. Qian, L. Yang, C. Wang, Z. Chen, Mater. Sci. Eng. B49 (1997) 42.

[28] S. Lian, E. Wang, L. Gao, L. Xu, Mat. Letters, 61 (18) (2007) 3893.

[29] M. Cao, C. Hu, Y. Wang, Y. Guo, C. Guo and E.B. Wang, *Chem. Commun.* 1884 (2003).

[30] J. B. Goodenough and A. L. Loeb, Phys. Res.. 982 (1955) 391.

[31] R. C. Weast, Handbook of Chemistry and Physics, 57th Ed., CRC Press, Inc., 1976-1977.

[32] M. G. El-Shaarawv and T. El-Assawy, J.Mater. Chem. Phys., 62 (2000)1.

[33] V. Biju and M. Abdul Khadar, Mater. Sci. Eng. A, 304-306 (2000) 814.

[34] M. Pollak and Y.H. Gaballe, Phys. Rev., 122 (1961) 1742.

[35] S. R. Elliott, Adv. Phys., 36 (1987) 135.

[36] S. Mørup, M.F. Hansen, C. Frandsen, Magnetic Nanoparticles,Comprehensive Nanoscience and Technology,(2011), Chapter 1.14, Pages 437-491.

[37] R. K. Gupta, K. Ghosh, L. Dong, P.K. Kahol , Mat. Letters, 65 (2) (2011) 225.

[38] P. Priyadharsini, A. Pradeep, P. Sambasiva Rao, G. Chandrasekaran, Mater. Chem. and Phys., 116 (1), (2000)207.

[39] T. K. Pathak, N. H. Vasoya, V. K. Lakhani, K. B. Modi, Cer. Inter., (36) (1) (2010)275.

[40] V. Kumar, A. Rana, M.S. Yadav, R.P. Pant, J. Magn. Magn. Mater., 320 (1)(2008)1729.